



INFLUENCE OF IMPELLER SUCTION SPECIFIC SPEED ON VIBRATION PERFORMANCE

David Cowan

Hydraulics Engineer
ITT Goulds Pumps
Basingstoke, Hampshire, UK

Thomas Liebner

Hydraulics Engineer
ITT Goulds Pumps
Seneca Falls, NY, USA

Simon Bradshaw

Director of API Product Development & Technology
ITT Goulds Pumps
Seneca Falls, NY, USA



David Cowan is a Hydraulics Engineer with ITT Goulds Pumps responsible for applied research and hydraulic design of engineered API process pumps. His responsibilities include the development and analysis of new and existing hydraulic products through traditional and computational methods. He is also jointly responsible for continuous development of the computational fluid dynamic analysis techniques. Prior to joining ITT Goulds, he worked as a Hydraulic Engineer for ClydeUnion Pumps.

Mr. Cowan has a B.Sc. in Aeronautical Engineering from the University of Glasgow.



Thomas Liebner is a Hydraulics Engineer with ITT Goulds Pumps responsible for applied research and hydraulic design of engineered API process pumps. His responsibilities include – new product design, computational modeling, and hydraulic analysis for performance prediction.

Dr. Liebner has a B.S. in Mechanical and Aerospace Eng. from SUNY at Buffalo. He completed his studies for his doctorate in Mechanical Engineering at Penn State University where he performed experimental and computational modeling of particle adhesion and their liberation and entrainment in air jets.



Simon Bradshaw is the Director of API Product Development & Technology for ITT Goulds Pumps, in Seneca Falls NY. His responsibilities include the design and development of new products and processes. Prior to joining ITT Goulds, he worked for both Sulzer Pumps and Weir Pumps, where he held various positions of engineering and contractual responsibility. Additionally he has supported the Hydraulic Institute in the development of pump standards and best practice guides.

Mr. Bradshaw has a BEng (Hons) degree (Mechanical Engineering) from Heriot Watt University. He is a registered Chartered Engineer in the UK and a member of the Institute of Engineering Designers.

ABSTRACT

The most commonly used hard limitation for pump suction specific speed is 11,000 (US units). This hard limit grew out of the recommendations from a 1982 reliability study by J.L. Hallam (Hallam 1982). Concomitant testing of the vibration performance of an OH2 4x6-11 pump was made with impellers designed for different suction specific speeds (Lobanoff and Ross 1985). This study showed that all things being equal, a strong relationship existed between suction specific speed and the pump vibration at off BEP operation.

Given the significant changes in impeller design methods and computational tools in the subsequent three decades, this paper seeks to investigate how these new methods/tools have affected the relationship between suction specific speed and the pump vibration.

Experiments are performed using a series of impellers designed for different suction specific speeds using modern design techniques. These impellers are mounted in a subject test pump which is also an OH2 4x6-11 in order to achieve equivalency with the prior testing. Vibration performance over the pump operating range is recorded. The results are complemented with computational fluid dynamic (CFD) analysis to further examine the performance of each impeller.

BACKGROUND

The suction performance of a centrifugal pump is an extremely important consideration for optimal pump performance. Good suction performance allows for the use of smaller piping, lower tank elevations, less excavation and a general optimization of plant design. These optimizations can lead to significant 1st cost savings.

In the 1950's to 1980's the impeller design methods available to pump designers were more limited than they are today. Impeller designs from that era were notable for their achievement of good suction performance through the deployment of large impeller inlet diameters (D1). It was not understood until later that the enlarging of the impeller inlet diameter caused impairment of the impeller performance at flow rates lower than the best efficiency point (BEP). This impairment exhibited itself as significantly increased vibration and in some extreme cases an unstable NPSHr characteristic.

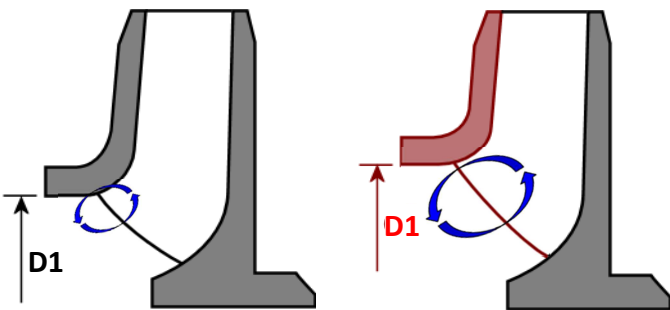


Figure 1a: Effect of larger D1 on suction recirculation strength

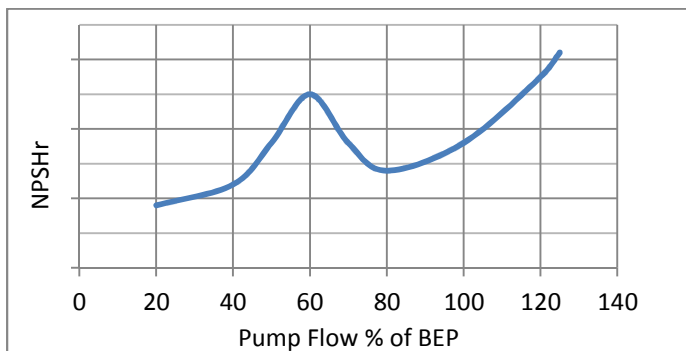


Figure 1b: Unstable NPSHr characteristic.

The landmark paper by Warren Fraser (Fraser 1981), brought the consequences of relying on large impeller inlet diameters into focus. Pump users had already become increasingly concerned that while such designs minimized plant 1st cost, it was at the price of reliability and overall life cycle cost. However, there was no large scale study available of the phenomenon in an actual pump population and hence the nature of the trade-off between suction performance and reliability was unclear.

This changed when Jerry Hallam (Hallam 1982) published the results of a large scale reliability study of 480 pumps over a 5 year period at the Amoco Texas City refinery. He found that the reliability of a pump was meaningfully related to its suction specific speed (N_{ss}). Specifically pumps with a N_{ss} > 11,000 (S > 213) failed twice as often compared to lower suction specific speed pumps. Figure 2 shows the failure rate vs. suction specific speed.

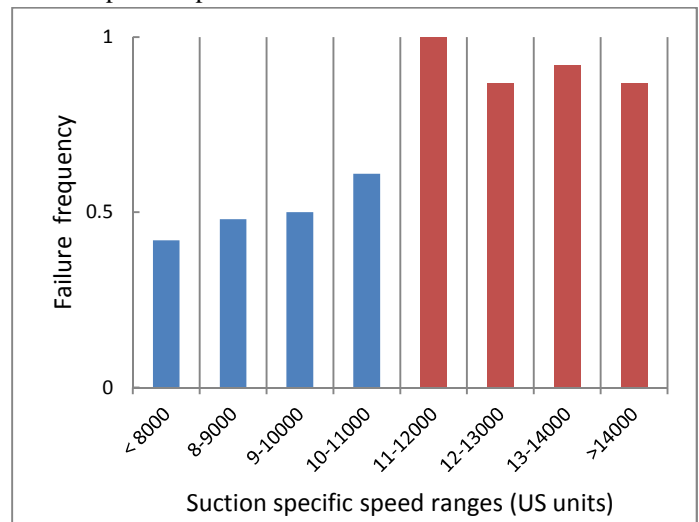


Figure 2: Failure frequency vs. suction specific speed.

Hallam concluded: "This study indicates that caution should be exercised when purchasing hydrocarbon or small water pumps with a N_{ss} greater than 11,000 unless operation is closely controlled near BEP."

This conclusion was supported by the results of testing an OH2 configuration 4x6-11 (100x150-280) pump in the book Centrifugal Pumps: Design & Application (Lobanoff and Ross 1985). For this testing a series of eight impellers with differing suction specific speeds were designed and tested at 3560 RPM. The range of suction specific speeds varied from N_{ss} = 7000 (S = 135) to N_{ss} = 20,000 (S = 387). For each impeller the flow was varied until the pump vibration level exceeded the API 610 allowable level of 0.3 inches/sec (7.6 mm/s) peak. Those limiting flow rates are shown for each impeller in Figure 3.

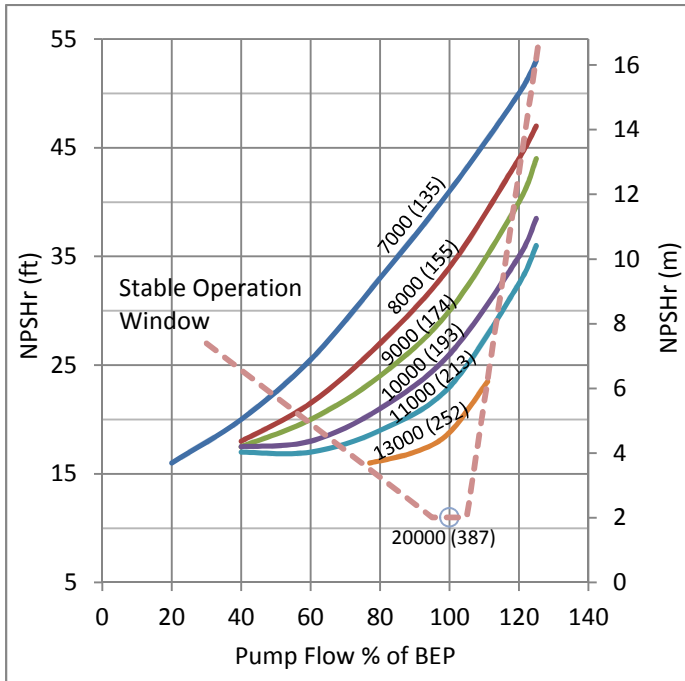


Figure 3: Stable window according to Lobanoff & Ross.

The testing showed that the impeller operating range with acceptable vibration characteristics was strongly related to suction specific speed.

In the years following the publication of Hallam's work the $N_{ss} = 11,000$ ($S = 213$) limit was widely adopted as a hard limit in the oil and gas industry to the extent that it is rare to see a specification that does not invoke it in some form. It is common to see the limit applied rigorously to the extent that (for example) a pump with $N_{ss} = 10,950$ ($S = 212$), is viewed as acceptable while a pump with $N_{ss} = 11,050$ ($S = 214$), is viewed as unacceptable.

A number of authors have over the years studied and reported that the influence of suction specific speed on pump reliability is diminished [(Stoffel and Jaeger 1996), (Hirschberger and James 2009), (Hergt et. al. 1996), (Gulich. 2001) and (Balasubramanian et al. 2011)]. Central to their claim was the premise that modern impeller design techniques, *ceteris paribus*, allowed attainment of higher suction specific speeds without resorting solely to enlargement of the impeller inlet diameter. However none of this work has altered the widespread view that the original $N_{ss} = 11,000$ ($S = 213$) number is the main criteria that should be used in assessing a pump's quality.

It is noticeable (by its absence), that there has been no similar follow-up large scale study of refinery pump reliability in the past 30 years. This is a concern given the increased emphasis on safety, life cycle cost and minimizing emissions.

INTRODUCTION

The purpose of this paper is to revisit the testing reported by Lobanoff and Ross in 1985. The reasons for doing so are primarily:

- changes to impeller design techniques, and
- improved design and construction standards.

Impeller design techniques

Impeller design techniques and tools have improved significantly in the last 30 years allowing impellers to attain a required suction performance while minimizing the increase in impeller inlet diameter. While not intended to be an exhaustive list, some of the design options available to today's designers include:

- Small incidence blade angles coupled with small blade and approach flow angles (for better NPSH behavior at part-load operation).
- Low blade loadings in the inlet region up to the impeller throat area. These help prevent the formation of low pressure zones where cavitation will begin.
- S shaped developments of the impeller camber line in order to achieve the required impeller throat area while minimizing the eye diameter.
- Backward swept blades to reduce the volume of any cavitation that develops at the leading edge.
- Impeller leading edge carried well forward at the impeller hub in order to reduce the formation of cavitation at part load operation.
- The deployment of better controlled leading edge profiles. These profiles effectively limit the leading edge pressure spikes and are less sensitive to part load operation. For example prior research by the author's company (Balasubramanian et al. 2011) has shown that optimized impeller leading edge profiles improve suction specific speed without requiring larger impeller inlets.
- Utilizing computational analysis techniques the impeller inlet design can be optimized for a given set of conditions, thus allowing greater control and understanding of the flow and pressure characteristics in the impeller passageway.

Design and construction standards

Pump standards (e.g. API 610 11th edition), have continued to evolve such that modern designs are more robust than designs existing in the 1980's.

Specifically, the L^3/d^4 ratio has been reduced in order to limit shaft deflection at the seal chamber to 0.002" (0.05mm) under any operating condition. L^3/d^4 is calculated from the impeller overhang (L) divided by the shaft diameter at the mechanical seal (d), see Figure 4. This mechanical constraint was driven by the need to improve mechanical seal reliability and the use of L^3/d^4 as a cost factor weighting representing life-cycle cost

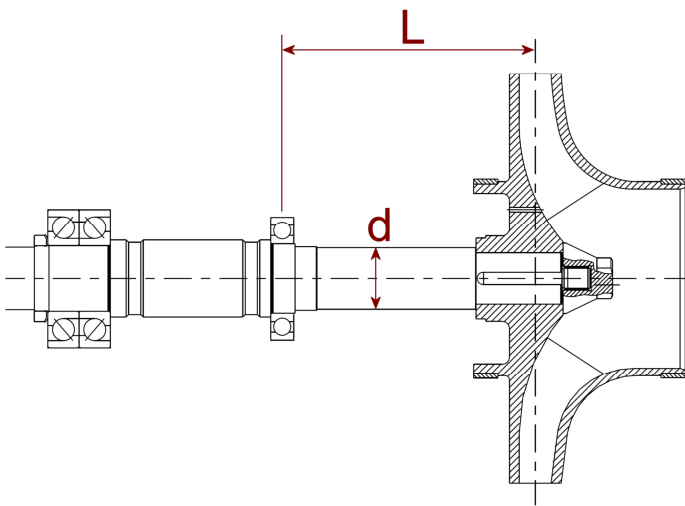


Figure 4: L^3/d^4 for an overhung pump rotor

It is not unusual to see pumps designed to earlier versions of API 610 having L^3/d^4 ratios that are 3x to 6x higher than the industry average today. For example in a comparison between the 4x6-11 (100x150-280) tested in this paper and a similar pump from a model line designed to an earlier version of API 610, the older design had a L^3/d^4 of 213 in^{-1} (8.4 mm^{-1}). This is 5x greater than the value of the pump tested for this paper which has a L^3/d^4 of 42 in^{-1} (1.65 mm^{-1}).

API 610 11th edition introduced non-binding criteria for L^3/d^4 in Appendix K of the standard. The criteria plots L^3/d^4 vs. a factor composed of the pump flow x head / speed. The location of the test pump is plotted on the graph in Figure 5 as compared with an older generation pump.

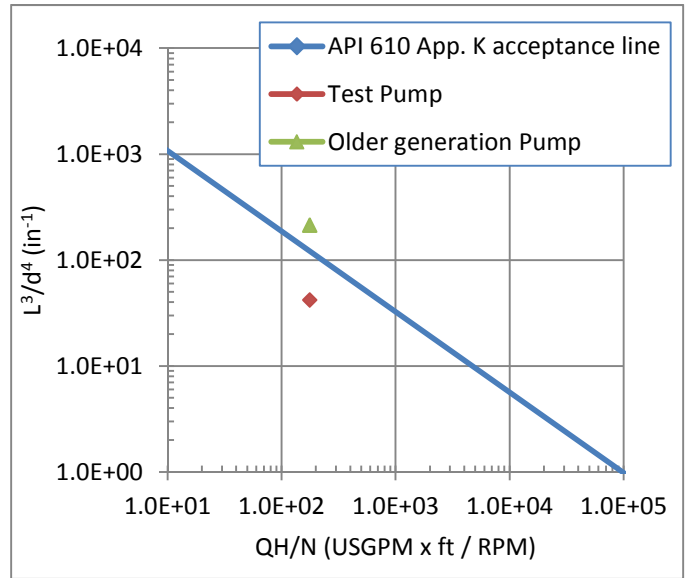


Figure 5: Excerpt from API 610 11th edition Appendix K

API 610 7th edition (1989) also introduced the current requirements for limiting the deflection of the pump under specified nozzle loads including optional testing. API 610 9th edition (2003) specifically prohibited the use of rear bearing housing supports on OH2 pumps. This required an improvement of the overall rigidity of the pump casing, bearing frame and baseplate.

Figures 6 and 7 contrast the arrangement of a casing foot typical of current designs with that of an older design. Consequently the improved rigidity tends to improve overall pump reliability and vibration performance.

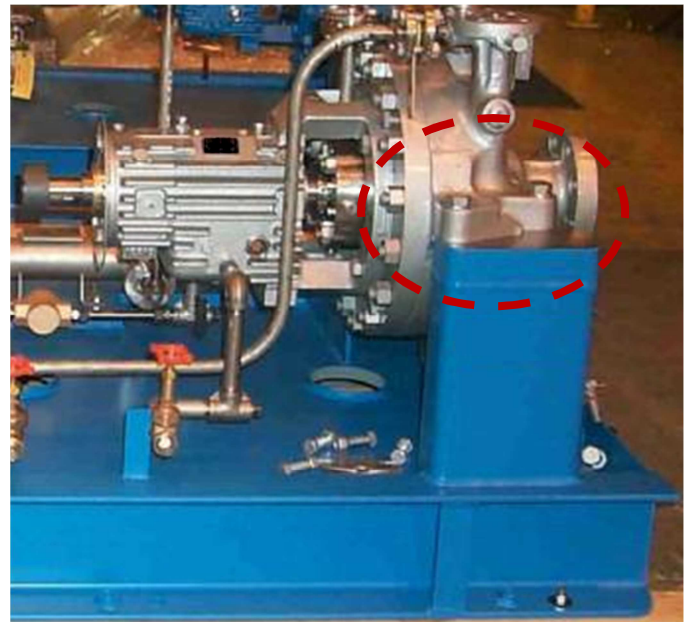


Figure 6: Pump foot fully compliant to API 610 11th edition.

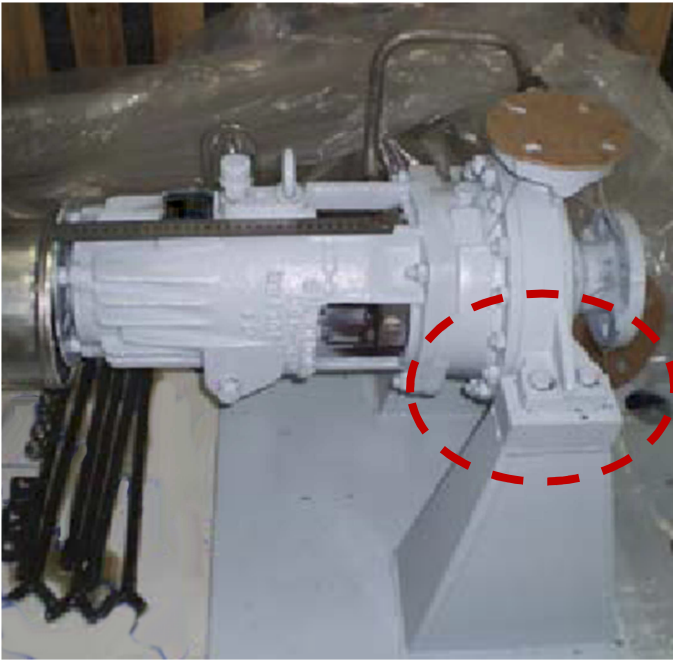


Figure 7: Pump foot design typical of a pump designed to pre-API 7th edition standards.

Hence it is timely to examine how these changes have affected the attainable acceptable flow range as it relates to suction specific speed.

TEST PUMP SETUP

The test pump selected is a 4x6-11 (100x150-280) in a single stage overhung configuration with centerline mount (OH2). It is fully compliant with 11th edition of API 610. In terms of overall construction it is unremarkable though consistent with the current best practice for a full compliant API 610 OH2 design. Figure 8 shows a cross-sectional view of the test pump.

The characteristics of the test pump are tabled below:

Parameter	Value
Running Speed	3560 RPM
BEP Head	450 ft (137 m)
BEP Flow	1670 USGPM (380m ³ /h)
BEP power @ 1.0 SG	232 HP (173 kW)
Specific Speed Ns (nq)	1489 (28.8)
Design Pressure	750 psig (51.7 barg)
Materials of Construction	API 610 code S6
Shaft dia. @ mechanical seal	2.362" (60mm)
L ³ /d ⁴ ratio	42 in ⁻¹ (1.65 mm ⁻¹)

Table 1: Test Pump Specifications

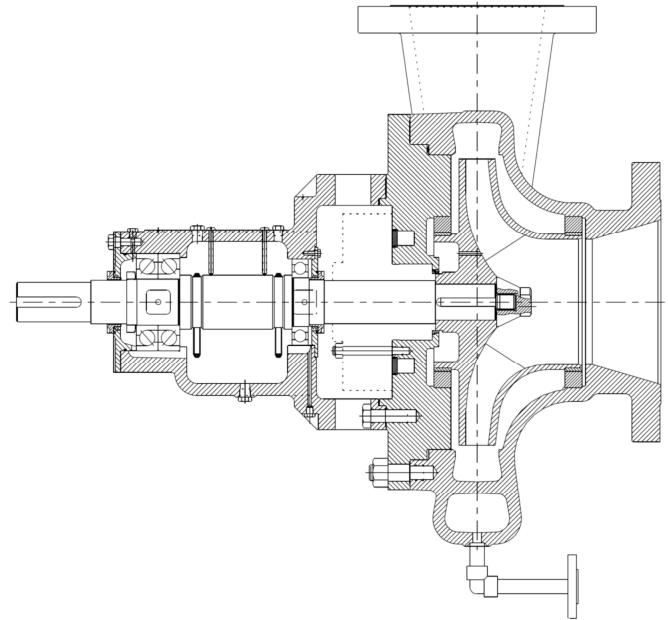


Figure 8: Cross-sectional assembly of the Test Pump

The pump was installed in a standard testing station in the large hot water tank (LHWT) test loop of company’s R&D facility. The test setup complied with HI 14.6 test standards. Figure 9 shows the test pump as installed in the test loop. It is important to note that all test loop setups are temporary constructions and the vibration levels measured on the pump will necessarily be higher than those achieved in the final site installation. The absence of a large permanent foundation and grout reduces the ability of the test setup to attenuate these vibrations effectively. Additionally, all of the fluid energy imparted by the pump needs to be dissipated within the test loop. This tends to cause vibrations that are fed back to the pump, and in extreme cases acoustic resonances can occur in the typically short pipe runs.

Hydraulic Institute recognizes this fact in their vibration standard 9.6.4 which has higher allowable levels for factory testing than for site testing. API 610 makes no such distinction and requires the same low levels be achieved in the factory test loop as in the final permanent site installation.



Figure 9a: Pump installed in the test loop



Figure 9b: Pump installation (bearing housing view)

For the purposes of the testing, the following allowable vibration levels were used in accordance with API 610 11th edition:

Parameter	Vibration level
Overall unfiltered in the flow range 70% to 120% of BEP	0.12 in/s (3.0 mm/s)
Any discrete frequency in the flow range 70% to 120% of BEP	0.08 in/s (2.0 mm/s)
Overall unfiltered in the flow range MCSF to < 70% and > 120% of BEP	0.156 in/s (4.0 mm/s)
Any discrete frequency in the flow range MCSF to < 70% and > 120% of BEP	0.10 in/s (2.6 mm/s)

Table 2: Vibration criteria for acceptable performance under API 610 11th edition.

These vibration values would be used to determine the allowable operating range of each impeller.

IMPELLER DESIGN

For the test rig, four single entry end-suction impellers were designed. Details of the key geometry information are tabled below. Constraints were placed on the maximum outlet width dimension to ensure each impeller could fit within the standard 4x6-11 case being utilized as well as ensuring similar radial thrust values.

The impellers were designed with varying suction specific speed (N_{ss}) constraints, notably 8000 through 15000, with the intent to maintain a standard generated head and best efficiency flow rate.

Maintaining a similar meridional geometry between impellers is not possible due to the large increases in suction specific speed. As such, the impeller eye diameters gradually increase causing differences in the overall meridional shape.

There was some variation in discharge angle and discharge width between the different designs. B_2 and β_2 are strongly dependent, and were adjusted to achieve the appropriate discharge area while accommodating the variation in inlet geometry.

The inlet diameter for the highest N_{ss} impeller was almost 20% larger than the lowest N_{ss} design. An overlay of each of the impeller meridional shapes can be seen in figure 10.

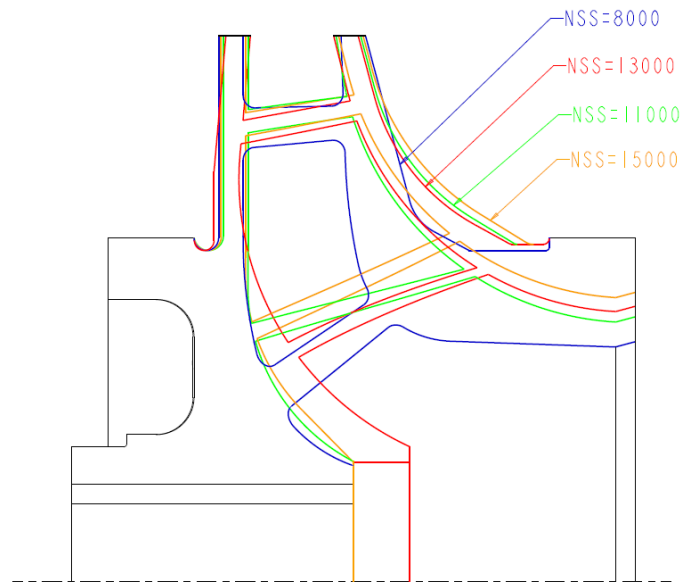


Figure 10: Overlay of meridional geometries

	Design 1	Design 2	Design 3	Design 4
Nominal Nss (S)	8000 (155)	11,000 (213)	13,000 (252)	15,000 (290)
D ₂ Impeller outlet diameter (in)	11	11	11	11
B ₂ Impeller outlet width (in)	1	0.9	0.85	0.95
β ₂ Impeller vane angle @ outlet (deg)	24	26.3	29	27.5
D ₁ Impeller inlet eye diameter (in)	4.9	5.3	5.5	5.8
β ₁₁ Impeller vane angle @ inlet (deg)	29	13.2	14.7	11.7
D ₁ / D ₂ Impeller inlet / impeller outlet dia.	0.44	0.48	0.5	0.53

Table 3: Basic dimensions for the four impeller designs.

As discussed previously, in research by the authors company (Balasubramanian et al. 2011), it was demonstrated that cavitation is better controlled and higher Nss values achieved by employment of optimized leading edge profiles. As such, a parabolic leading edge profile was adopted for each of these designs, but the benefit of the leading edge profile was not considered in the impeller design calculations (and impeller design system utilized for these designs), as the exact improvement that could be realized was uncertain.

To reduce variability between the impellers, a constant wear ring diameter has been used. Wear ring clearances were in conformance to API 610 11th edition Table 6.

In standardizing the wear ring geometry the consequential volumetric loss is constant across the four impellers. This ensures a standard fluid damping effect. Wear ring length has been held constant across the impellers to normalize the favorable centering “Lomakin” effect. While API 610 does not allow this effect to be considered when calculating the shaft deflection, it does provide some additional stiffness and damping and hence it was necessary to keep it constant for all impeller designs.

The impellers were manufactured directly from the 3D model using rapid investment casting techniques (pattern less manufacture) and the cast impellers using SLA rapid prototyping process. Pictures of the resulting impellers are shown in Figures 11a to 11d

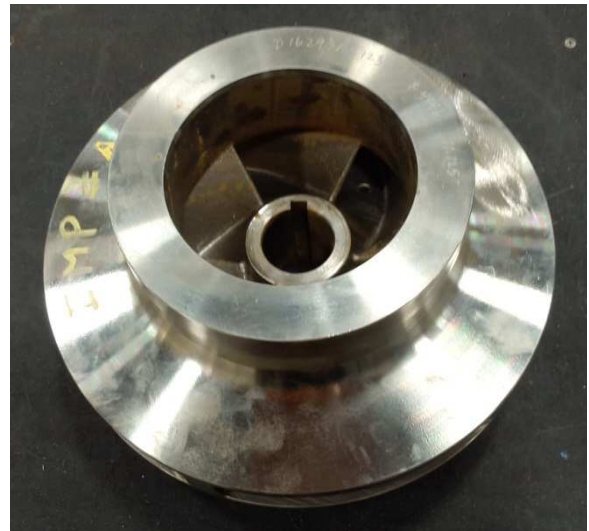


Figure 11a: Nss= 8000 nominal impeller



Figure 11b: Nss= 11000 nominal impeller



Figure 11c: Nss= 13000 nominal impeller



Figure 11d: Nss= 15000 nominal impeller

COMPUTATIONAL FLUID DYNAMICS (CFD)

To verify the hydraulic designs, a computational study, conducted within the framework of the ANSYS-CFX solver, [ANSYS CFX-14.5, 2012], was undertaken. The initial motivation for the computational analysis was to ensure that each design achieved its target Nss at the best efficiency point (BEP) while maintaining comparable performance. Additionally, the CFD results can provide insight into the development of cavitation on the leading edge of the blade and into the onset of recirculation within the impeller. The onset of suction side recirculation as the flow rate through the impeller is reduced should signal an increase in vibration characteristics.

For simplicity, a single blade-centered passage with a steady-state flow condition was utilized for this analysis. This has certain limitations as it neglects the effect of the casing and any unsteady characteristics including blade pass and system response. However, it makes the size of the mesh and the time to convergence manageable such that multiple flow conditions could be analyzed.

MESH STRUCTURE

An unstructured mesh with tetrahedral mesh elements was generated using the Simmetrix grid generation software [Simmetrix MeshSim, 2012]. A boundary layer mesh with hexahedral mesh elements was placed on wall surfaces. A minimum Δy was established such that the average y^+ value on the vane surface was between 10-20. The $k-\omega$ model with the shear stress transport (SST) adaptation is utilized to model the turbulence and near-wall structures. For this turbulence model, a y^+ of less than 30 has produced repeatable results while sufficiently capturing the near-wall characteristics. The global

size is chosen as 0.015x the maximum length of the passage. This allowed for an average of 5 cells across the width of the passage. The mesh size for the four models varied between 450,000 and 600,000 nodes.

A grid refinement study was performed for one of the design cases to ensure that the mesh was properly constructed and would produce results of sufficient accuracy. Three meshes of increasing refinement were utilized. The results of this sensitivity study are described in table 4.

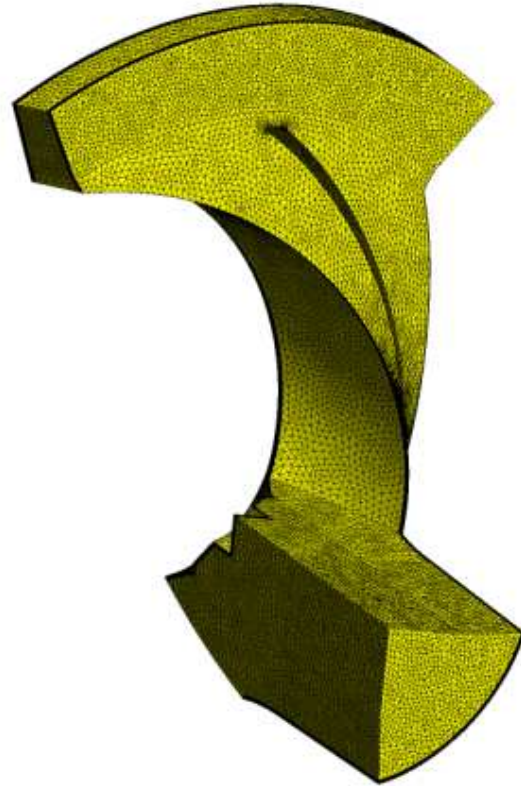


Figure 12. Sample mesh used during computational study.

As described in the book Centrifugal Pumps by Johann Gülich, approximating a grid independent solution (H_{nu}), the discretization errors (e_h) and the order (p) of the solution can be calculated utilizing solutions of grid sizes that differ by a factor of 2. The equations are listed below.

$$p \approx \frac{1}{\log 2} \log \left(\frac{H_h - H_{4h}}{H_h - H_{2h}} \right)$$

$$e_h = \frac{H_h - H_{2h}}{2^p - 1}$$

$$H_{nu} \approx H_h + \frac{H_h - H_{2h}}{2^p - 1}$$

Mesh Size	Predicted Head	Predicted 3% NPSHr
Nodes	H _o / H _{nu}	NPSHr/NPSHr _{nu}
164,000	1	1.19
332,000	0.99	1.05
590,000	1	1.01
p	-2	-2
e _h	5.33	-2.67
H _{nu} / NPSHr _{nu}	509.3	13.83

Table 4: Mesh refinement sensitivity study

CFD SOLVER CRITERIA

The analysis of the four designs was performed utilizing the ANSYS-CFX solver. The homogeneous two-phase mixture model is employed to model cavitation. The cavitation model is based on the Rayleigh-Plesset equation with source terms for the generation and destruction (vaporization and condensation) of vapor bubbles [Bakir et al., 2004]. The model solves for two-phases, vapor phase (α_{vapor}) and liquid phase (α_{water}), at each control volume location, with the sum of both phases equal to one ($\alpha_{\text{vapor}} + \alpha_{\text{water}} = 1$) at each location. The basic assumption of the model is that all phases share the same velocity and a mixture equation is solved for the conservation of momentum. High resolution fluxes are chosen for the discretization of mean flow and turbulence equations. The shear stress transport (SST) turbulence model is used for modeling turbulence.

Simulations are performed for a single passage of the impeller geometry as shown in Figure 13. For the analysis, no slip boundary conditions are applied at the hub, shroud and blade; total pressure is set at the inlet with the volume fraction of water as 1.0 and vapor as 0.0; mass flow rate is specified at the exit; and rotational periodicity is applied at the periodic interfaces (passage boundaries) as shown in Figure 7.

Convergence for the velocity and momentum residuals was determined below an RMS value of 10^{-4} . Each of the trial runs required between 200 and 400 iterations to achieve convergence.

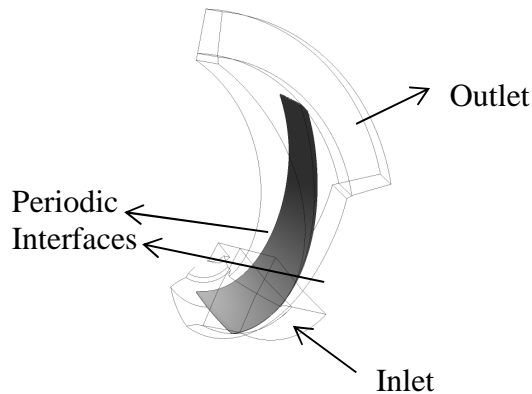


Figure 13: Single-passage CFD model for analysis

Multiple runs were conducted for each of the impellers. Four different flow rates were investigated at 60%, 80%, 100%, and 120% of the target best efficiency point (BEP) for each of the four designs. At each of these flow rates, the inlet total pressure was gradually reduced to compute the head drop performance curves, essentially simulating a typical NPSH test run. Figure 14 demonstrates a typical head drop curve predicted by the computational analysis.

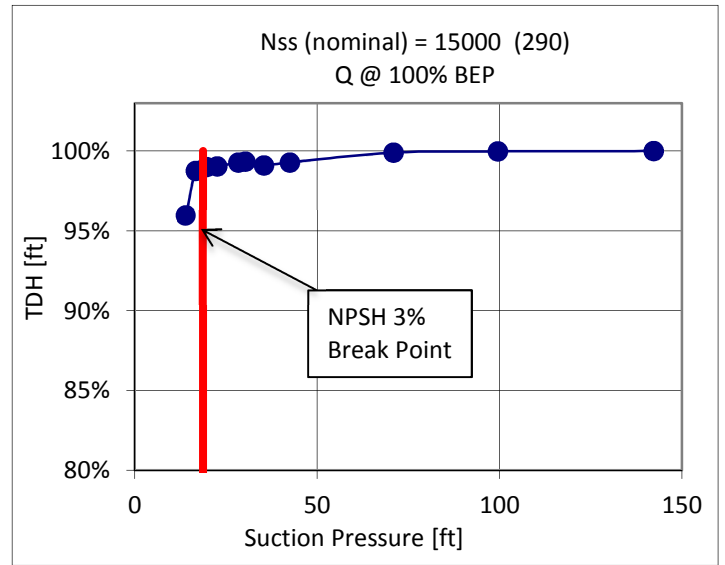


Figure 14: Typical head breakdown curve

PREDICTION OF RECIRCULATION BY THE FRASER METHOD AND CFD

Warren Fraser (Fraser 1981), provides an estimate for the onset of suction recirculation within centrifugal pumps based on major dimensions within the impeller. The equation for this is shown below. There is mention made in the paper that the equation was developed using observations of suction recirculation in a special test pump equipped with a transparent suction pipe. It is not clear from the paper as to exactly how observations made on test pumps were correlated with the resulting formula. Specifically there is no mention as to how extensive the recirculation zone must be to assure experimental observation. This makes it difficult to correlate with the CFD determinations of the recirculation zones.

$$Q_{suct\,recirc} (US\ units) = \frac{D_1(D_1^2 - h_1^2)N}{93.45} * \frac{v_e}{u_1} \quad \text{for } D_1/D_2 > 0.5$$

Thus for the purposes of comparison the impeller under CFD analysis is deemed to be recirculating when the recirculation zone extends upstream of the leading edge of the

impeller vane, which presumably would have been observable in Warren Fraser’s test pump.

For each impeller design, single phase CFD runs were performed where the flow rate was reduced in 5% increments from BEP. Figures 15a to 15d show samples of the resulting output. The results were compared for each impeller and a determination made regarding the flow at which recirculation extended beyond the vane leading edge. This flow rate was deemed to be “recirculation onset”

Predictions for the onset of recirculation are shown in Table 5 for both methods. The flowrate at which suction side recirculation occurs increases with increasing suction specific speed. This is to be expected as the higher suction specific speed impellers have larger impeller inlet eye (D1) diameters.

It can be seen that the values predicted by CFD and Fraser’s equation show substantive agreement. This appears to validate the choice of CFD recirculation criteria.

Nominal Suction Specific Speed	Fraser Suction Recirc. (% of BEP)	CFD Suction Recirc. (% of BEP)
8000 (155)	48%	≈48%
11,000 (213)	60%	≈63%
13,000 (252)	66%	≈63%
15,000 (290)	75%	≈74%

Table 5: Recirculation predictions based on Fraser & CFD

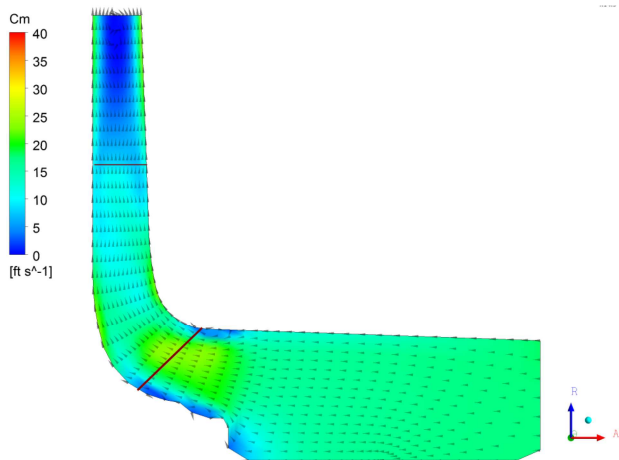


Figure 15a. Small recirculation cell ahead of vane at 50% BEP Flow, 8000 Nss (S=155) design.

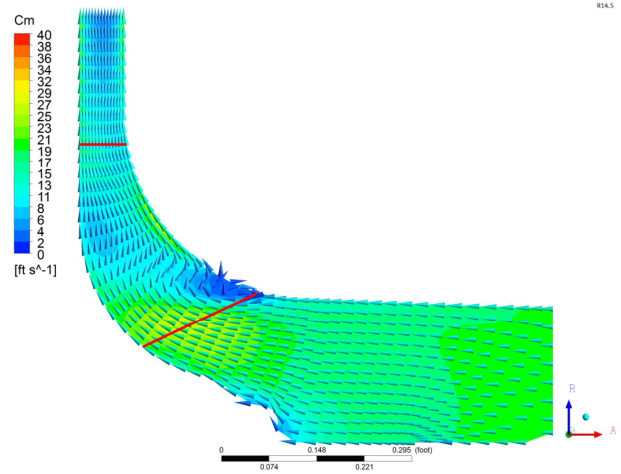


Figure 15b. Recirculation cell ahead of vane at 65% BEP Flow, 11,000 Nss (S=213) design.

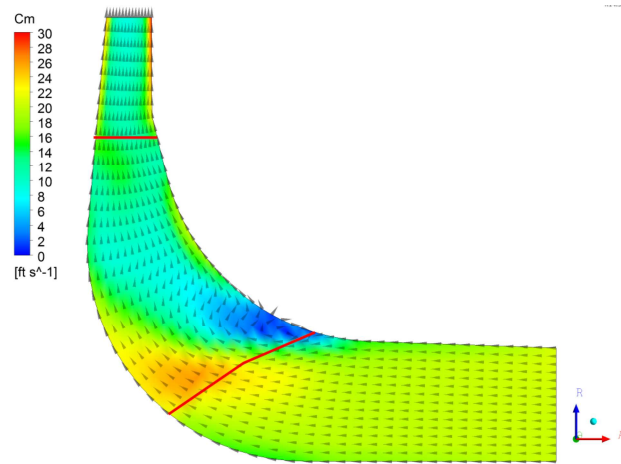


Figure 15c. Recirculation cell ahead of vane at 65% BEP Flow, 13,000 Nss (S=252) design.

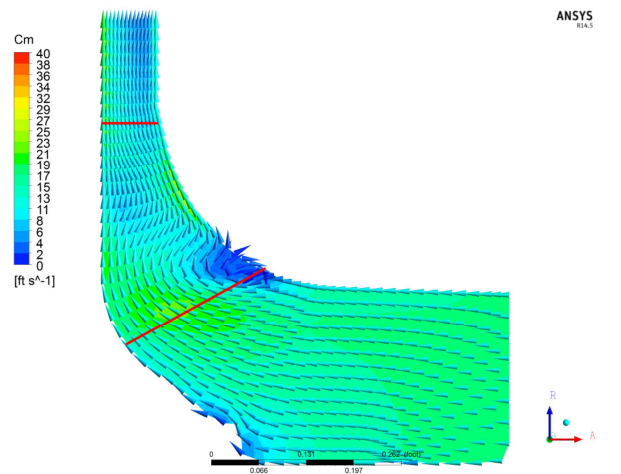


Figure 15d. Recirculation cell ahead of vane at 75% BEP Flow, 15,000 Nss (S=290) design.

EXPERIMENTAL RESULTS

Each impeller was subject to a full performance and NPSH test based on the criteria set out in API 610. The results of each impeller performance compared to the design target are shown in Figures 16 and 17. These results confirmed the prediction of the CFD. Head and efficiency agreed within 5% between CFD and test when the calculated casing losses were combined with the CFD values.

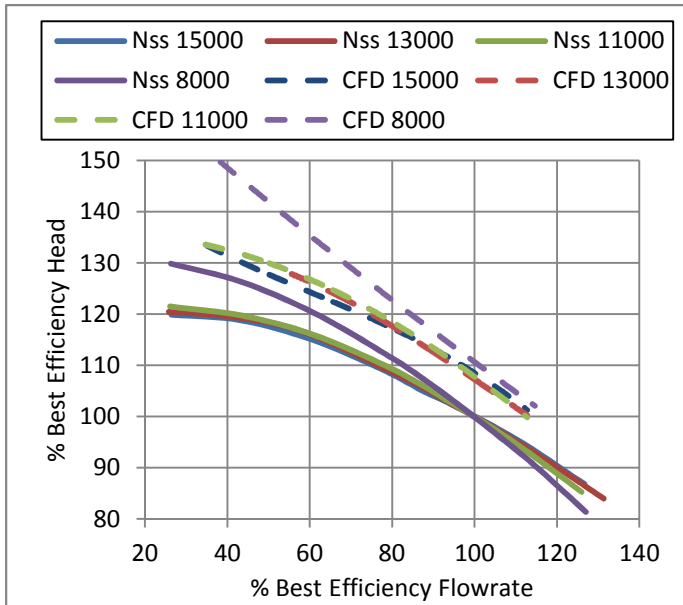


Figure 16: Experimental Testing and CFD analysis (note the CFD results show the impeller performance only.)

Tested NPSHr was 21% to 33% lower than the original nominal target values. These values and the corresponding suction specific speed are shown in Table 7.

Nominal Suction Specific Speed	Target NPSHr @BEP ft (m)	Tested NPSHr @ BEP ft (m)	Tested Suction Specific Speed
8000 (155)	47.8 (14.6)	37.4 (11.4)	9568 (185)
11,000 (213)	31.3 (9.5)	21.1 (6.4)	14,776 (286)
13,000 (252)	25.0 (7.6)	17.6 (5.4)	17,066 (331)
15,000 (290)	20.7 (6.3)	16.4 (5.0)	17,841 (346)

Table 7: Nominal target vs. tested NPSH and Nss

There are two main reasons for this difference:

1. The acceptance tolerance for NPSHr allows no positive tolerance. Thus impellers are designed to achieve lower than the target NPSHr by approximately 14% to allow for manufacturing variances and uncertainty of design.
2. The design methods used did not take into account the improvement achieved through use of the parabolic

leading edge profile. From previous testing this NPSHr improvement was believed to be approximately 18%.

In addition to comparing the target NPSHr values with the tested values, the tested NPSHr values were compared to the CFD simulation.

For flow values higher than the onset of suction recirculation, the values of NPSHr from CFD showed substantive agreement with the tested NPSHr values. NPSHr predictions obtained via CFD are typically 5-15% lower than those attained on test. This can be accounted for with casting and surface imperfections, unsteady flow features including vane pass contributions and system response characteristics, and non-uniform inlet flow fields

At lower flow rates the tested NPSHr values diverged from the CFD predicted NPSHr values due to impeller-casing interaction in recirculation which the impeller only CFD is unable to simulate. Results of predicted 3% head drop versus flow are shown in Figures 17a and 17b below.

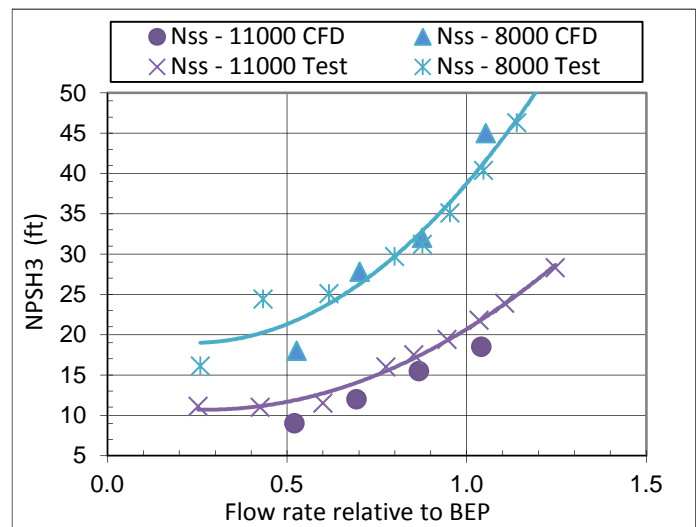


Figure 17a: Computational & test results for 3% NPSHr (8000 and 11,000 nominal Nss impellers)

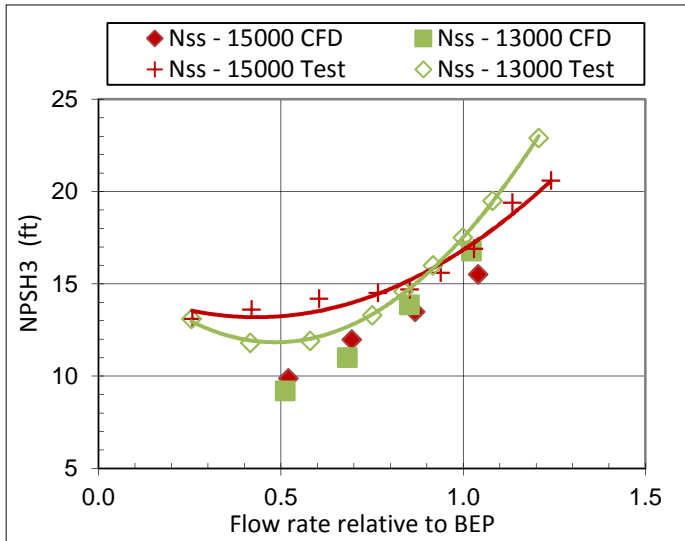


Figure 17b: Computational & test results for 3% NPSHr (13,000 and 15,000 nominal Nss impellers)

Vibration values for the both overall vibrations and vane pass are plotted on Figures 18 and 19. (Vibration levels due to mechanical sources, specifically 1x and 2x running speed were less than the 0.08 in/s (2.0 mm/s) allowable level for discrete frequencies and were therefore not used as an acceptance criteria).

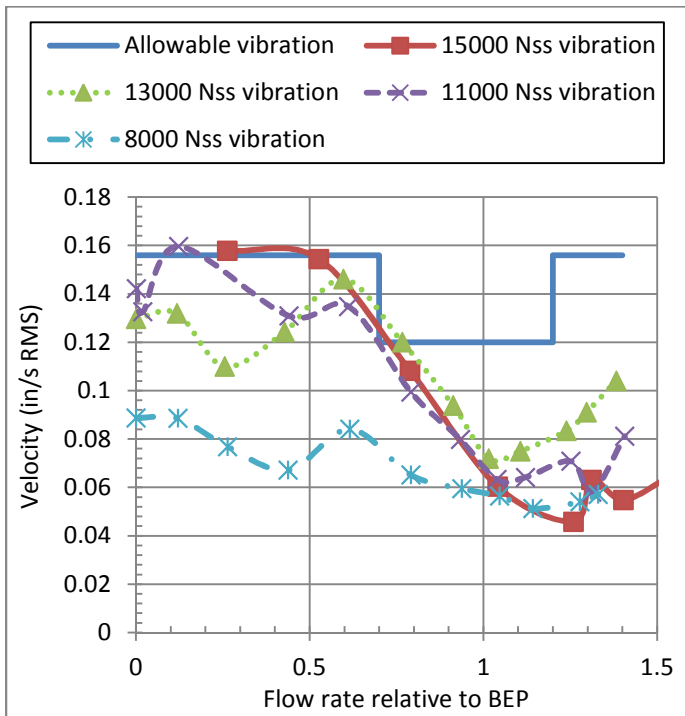


Figure 18: Overall vibration level on test.

The results show that all impellers exhibit a rising vibration level away from the impeller shock-less flow point. The Nss 15,000 nominal (17,841 actual) impeller design

exceeded the acceptable vibration level at 86% of BEP due to vane pass.

The 13,000 nominal (17,066 actual) impeller design exceeded the acceptable vibration level at 76% of BEP due to vane pass.

The 11,000 nominal (14,766 actual) and 8000 nominal (9568 actual) impeller designs did not exceed any vibration criteria throughout the entire operating range tested from 25% to approximately 140% of BEP.

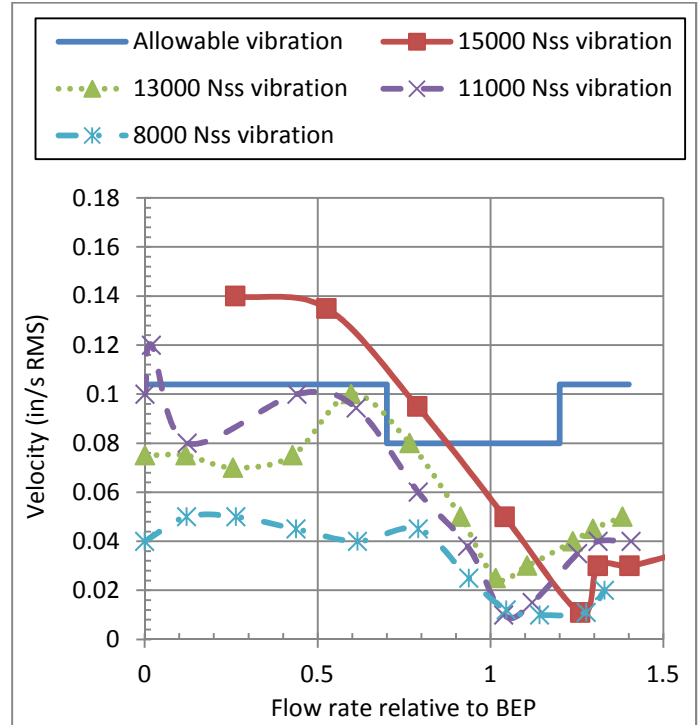


Figure 19: Vane pass frequency vibration level on test.

It should be noted that the test setup was of average quality. The test pedestals were clamped to the test base and were not specifically designed for the pump being tested. Consequently the vibration levels achieved could be meaningfully improved by refinement of the test setup. Similarly for a pump permanently installed in the field on a grouted baseplate, we would also expect a reduction in vibration levels achieved on test.

The pump was also equipped with a suction tapping adjacent to the eye of the impeller (see Figure 20). The pressure at this tapping was logged and compared to the pressure at the suction tapping at a location 2D in front of the suction flange. The purpose of this measurement was to ascertain when suction recirculation occurred and compare this result with the values predicted by Fraser and CFD.

Figure 21 shows a plot of suction pressure recorded at both tappings, normalized for the area differences and corrected for friction losses between the two locations. This shows an apparent recirculation inflection point for all the designs between 60% and 70% of BEP as shown in Table 8.



Figure 20: Location of the casing suction tapping.

While the tapping clearly records the presence of suction recirculation, the number of readings taken and their scatter precluded this method from providing an accurate indication of the onset of recirculation. As can be seen from Table 8, there was significant disagreement between the both Fraser and CFD as compared to the values obtained during this test.

With more time and refinement of the technique (in particular a much higher density of measurement points), we believe it could yield a more accurate indication, however for the purposes of this paper the technique will not be discussed further.

Nominal Suction Specific Speed	Fraser Suction Recirc. (% of BEP)	CFD Suction Recirc. (% of BEP)	Test Suction Recirc. (% of BEP)
8000 (155)	48%	≈48%	≈62%
11,000 (213)	60%	≈63%	≈65%
13,000 (252)	66%	≈63%	≈67%
15,000 (290)	75%	≈74%	≈64%

Table 8: Recirculation recorded on test & compared to the predictions from Table 5.

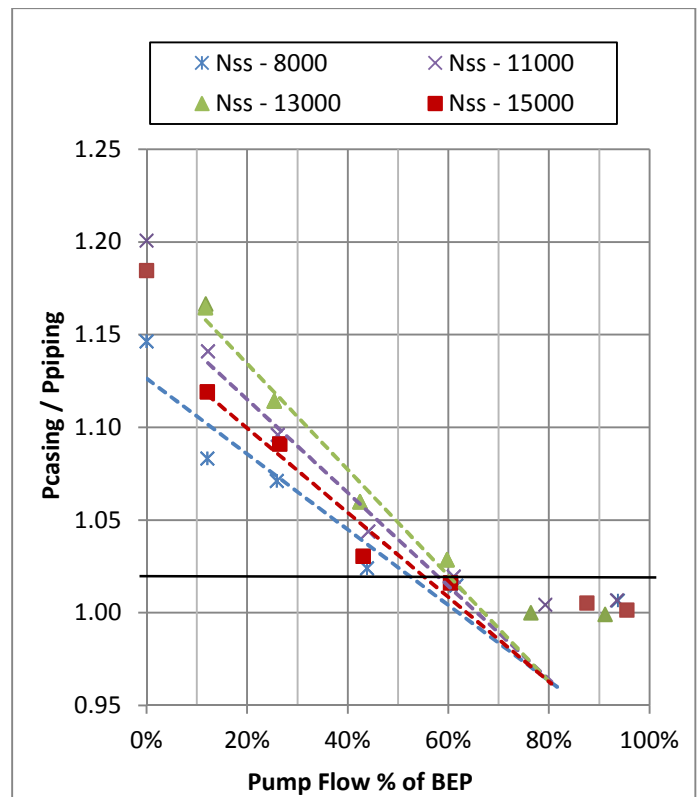


Figure 21: Ratio of suction performance at casing to upstream in the suction pipe.

DISCUSSION

The test results can be converted into an operational range chart similar in style to that used by Lobanoff & Ross. Figure 22 shows this in detail. Compared to Figure 3, the stable operating window is substantively larger and only closes at suction specific speeds far above those typically specified by most users.

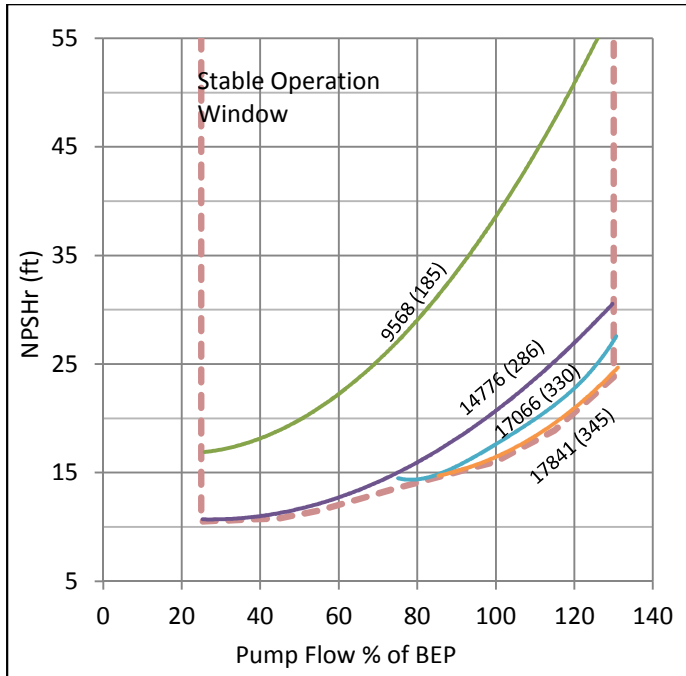


Figure 22: Stable operating window for the impellers tested

This result was compared to an existing internal guideline (known as the SGsT line), used by the author's company governing achievable end suction impeller designs with acceptable vibration and stability characteristics. This guideline is reproduced in Figure 23 with the impellers designed for this paper plotted on it. The main solid blue line indicates the dividing line between acceptable and non-acceptable performance.

For the specific speed of the test pump, the existing SGsT line value of approximately 13,000 nominal suction specific speed would appear to be easily attainable with the currently available design tools. As the state of the art continues to improve it may be possible to revise the SGsT line upwards in the future as shown on Figure 23.

It should be further noted that the SGsT line dips below 11,000 Nss for higher specific speed impellers. This is because at these higher specific speeds the ratio of impeller outlet diameter to impeller inlet diameter (D_2/D_1) is significantly reduced. As Warren Fraser (Fraser 1981) demonstrated, this ratio strongly determines when suction recirculation will occur.

Thus in order to achieve an acceptable operating range with these impellers, the Nss target needs to be reduced.

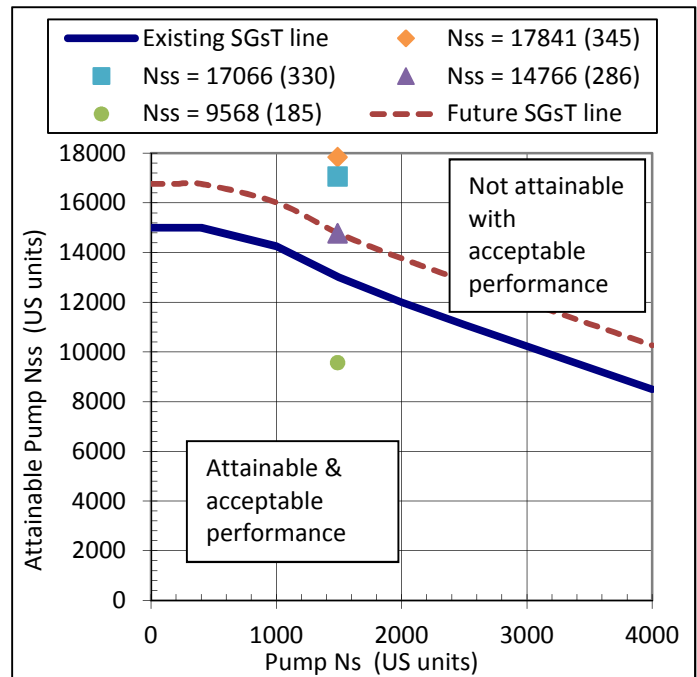


Figure 23: Trade off line (SGsT line) for Ns vs. Nss

SUMMARY AND CONCLUSIONS

The testing results confirm that substantive improvements in stable operating range vs. suction specific speed are achievable utilizing modern impeller design and pump construction standards. The realizable performance ($N_{ss} = 14,776$ ($S = 286$)) with acceptable vibration characteristics, is so far removed from what most users consider attainable that it should give pause for consideration as to whether $N_{ss} = 11,000$ is always the appropriate choice for medium to low specific speed impellers.

The authors would recommend that users consider adopting their own version of the SGsT line. The specific speed of the pump is an important determinant of the attainable Nss (with reliability) and needs to be recognized.

If correctly applied the use of such enhanced designs allow the designers of processes utilizing pumps, increased flexibility and the potential to realize a lower first cost with equal or even improved reliability (if high specific speed pumps are specified with conservative SGsT limits), than is possible with current one size fits all suction specific speed limit.

Of equal importance is action from the users of pumping equipment to build on Hallam's work and provide an updated large scale study of pump reliability for the 21st century.

NOMENCLATURE

BEP	= best efficiency point (flow rate) of the pump
CFD	= computational fluid dynamics
API	= American petroleum institute
$NPSH_A$	= available net positive suction head
$NPSH_3$	= net positive suction head at 3% head drop
$NPSH_r$	= net positive suction head required (= $NPSH_3$)
N_s	= specific speed (RPM, USGPM, ft)
N_{ss}	= suction specific speed (RPM, USGPM, ft)
S	= suction specific speed (RPM, m ³ /hr, m)
Q	= pump flow rate USGPM (m ³ /hr)
MCSF	= minimum continuous stable flow
D_1	= impeller eye diameter
β_1	= impeller vane inlet angle
D_2	= impeller outlet diameter
B_2	= impeller outlet width
β_2	= impeller vane outlet angle

REFERENCES

1. ANSYS-14.5 CFX Solver Theory Guide, 2012.
2. Hallam, J. L., Centrifugal Pumps: Which Suction Specific Speeds are Acceptable?, *Hydrocarbon Processing*, April 1982
3. Lobanoff, V.S., Ross, R.R., *Centrifugal Pumps: design & application 2nd Edition*, Figure 8-7
4. Gülich, J.-F., *Selection Criteria for Suction Impeller of Centrifugal Pumps, Parts 1 to 3 World Pumps January, March and April 2001*
5. Hergt, P., Nicklas, A., Mollenkopf, G., and Brodersen, S., 1996, The Suction Performance of Centrifugal Pumps Possibilities and Limits of Improvements, *Proceedings of the 13th International Pump Users Symposium, 1996*
6. Stoffel, B., Jaeger, R., 1996, Experimental Investigations in Respect to the Relevance of Suction Specific Speed for the Performance and Reliability of Centrifugal Pumps, *Proceedings of the 13th International Pump Users Symposium, 1996*
7. Hirschberger, M., James, I., 2009, A Review of N_{ss} Limitations – New Opportunities, *Proceedings of the 25th International Pump Users Symposium, 2009*
8. Balasubramanian, R., Bradshaw, S., Sabini, E., 2011, Influence of Impeller Leading Edge Profiles on Cavitation and Suction Performance, *Proceedings of the 27th international Pump Users Symposium 2011*
9. Schiavello, B., and Visser, F. C., 2008, Pump Cavitation – Various $NPSH_r$ Criteria, $NPSH_a$ Margins, and Impeller Life Expectancy, *Proceedings of the 24th International Pump Users Symposium, 2008*, Turbomachinery Laboratory, Department of Mechanical Engineering, Texas A&M University, College Station, TX.
12. Gülich, J.-F., *Centrifugal Pumps, Second Edition*

ACKNOWLEDGEMENTS

Special thanks to John Salerno (Jr.) for his help with all the necessary parts, Susan Sullivan for her successful impeller designs and: Denny Fenner, Marty Temple and Patricia BabowiczWebb for all their help with the extensive testing and data logging.